

Biological, Medical Devices and Systems

A Wearable Vital-signs Monitor at the Ear	123
A Portable Bioimpedance Spectroscopy Measurement System for Managing Congestive Heart Failure	124
A Subdermal EEG Monitor for Seizure Detection	125
An Electronically Steered, Wearable Transcranial Doppler Ultrasound System.....	126
Continuous and Non-invasive Blood Pressure Monitoring using Ultrasonic Methods	127
Body-coupled Communication and Implants	128
Automated Design of a Robust Decoupling Matrix for Multi-channel Parallel Transmit Coil Arrays in Magnetic Resonance Imaging	129
Ultimate Performance Metrics for Magnetic Resonance Imaging RF Coil Designs	130
Compact Dynamic Modeling for Large-Scale Cardiovascular System Simulation	131
Towards Wireless Capsule Endoscopic Ultrasound (WCEU)	132
High-Density, Three-Dimensional Microelectrode Arrays for Neural Recording.....	133
Reconfigurable Neural Probes for Chronic Electrical Recording.....	134
Thermal Drawing of Minimally Invasive Neural Probes	135
Size-based Biomolecule Preconcentration using Herringbone Nanofilter Arrays.....	136
Red Blood Cell Deformability and Splenic Clearance in <i>Plasmodium yoelii</i> Infected Mice	137
Microwell-based Platform For Single-cell Pericellular Protease Detection.....	138
Cell Pairing for Studying Immunity.....	139
Iso-dielectric Separation of Cells and Particles	140
Microfluidic Electronic Detection of Protein Biomarkers.....	141
Cell-based Sensors for Measuring Impact of Microsystems on Cell Physiology	142
Characterizing Deformability and Surface Friction of Cancer Cells.....	143

A Wearable Vital-signs Monitor at the Ear

E. Winokur, D. He, C.G. Sodini

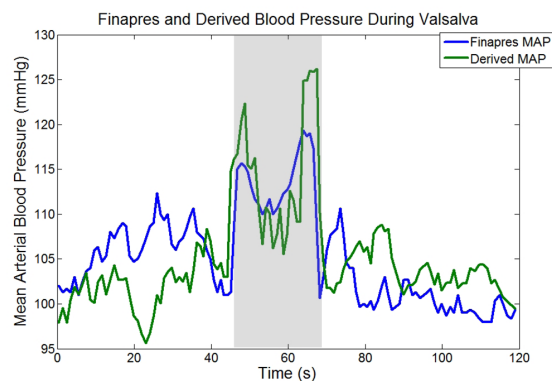
Sponsorship: Medical Electronic Device Realization Center, NSERC Fellowship

Vital signs such as heart rate, blood pressure, blood oxygenation, cardiac output, and respiratory rate are necessary in determining the overall health of a patient. Continuous monitoring of these vital signs can help healthcare workers assess the wearer's overall state of health and identify risks for cardiovascular diseases.

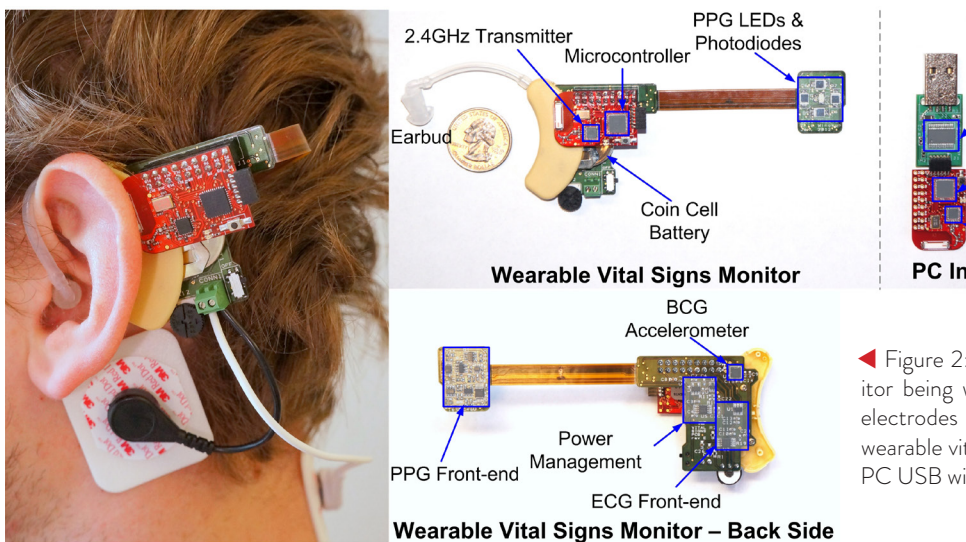
We propose a site behind the ear as a location for an integrated wearable vital signs monitor. This location offers physiological signals such as the electrocardiogram (ECG), the photoplethysmogram (PPG), and the ballistocardiogram (BCG). The ECG measures the electrical activity from the heart and offers heart rate information. The PPG measures the blood volume and color under the skin using optical illumination. The PPG offers information such as continuous heart rate and blood oxygenation. The BCG measures the body's mechanical reaction to the blood expelled by the heart and also provides the heart rate.

Using the peak timing data from BCG and PPG, the device can measure mean arterial blood pressure. Figure 1 compares the continuous mean arterial blood pressure measured from a Portapres finger-cuff with the continuous blood pressure measurement from the vital signs monitor while a test subject performed a Valsalva maneuver. The device is designed to use the

ear as a discreet and a natural anchor that reduces device visibility and the need for skin adhesives. A photo of our prototype device is shown in Figure 2. We have designed custom integrated circuits to reduce the form factor and lower the power consumption while still maintaining signal integrity in variable environments.



▲ Figure 1: A comparison of mean arterial blood pressure measured by a Portapres finger-cuff (blue) and mean arterial blood pressure derived from peak timing information of the vital signs monitor (green) during a Valsalva maneuver.



◀ Figure 2: Left - The vital signs monitor being worn at the ear with ECG electrodes attached. Center - The wearable vital signs monitor. Right - A PC USB wireless receiver.

FURTHER READING

- S. D. Pierdomenico, M. Di Nicola, A. L. Esposito, R. Di Mascio, E. Ballone, D. Lapenna, and F. Cuccurullo, "Prognostic value of different indices of blood pressure variability in hypertensive patients," *American Journal of Hypertension*, pp. 842-847, June 2009.
- D. He, E. S. Winokur, T. Heldt, and C. G. Sodini, "The ear as a location for wearable vital signs monitoring," *IEEE Engineering in Medicine and Biology Conference*, pp. 6389-6392, Sept. 2010.
- E. S. Winokur, D. He, and C. G. Sodini, "A Wearable Vital Signs Monitor at the Ear for Continuous Heart Rate and Pulse Transit Time Measurements," *IEEE Engineering in Medicine and Biology Conference*, pp. 2724-2727, Aug. 2012.

A Portable Bioimpedance Spectroscopy Measurement System for Managing Congestive Heart Failure

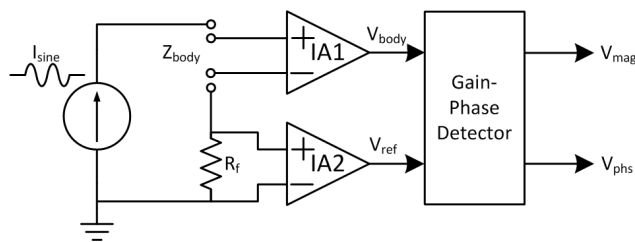
M. Delano, C.G. Sodini

Sponsorship: Medical Electronic Device Realization Center, Analog Devices

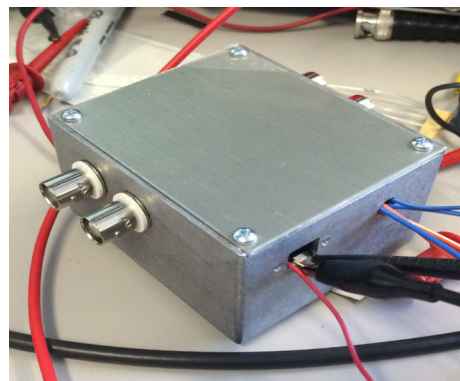
An estimated five million people are currently diagnosed with congestive heart failure (CHF) in the United States, with over 400,000 new diagnoses annually. CHF is frequently associated with significant fluid retention in the lungs and legs. Almost one in two patients will be readmitted to the hospital within four to six months of discharge. Readmissions can occur when the patient becomes fluid overloaded due to poor medication and/or diet compliance, among other reasons. Up to 50% of these early re-admissions may be prevented if symptoms are recognized early enough and medication/diet compliance improves.

Bioimpedance techniques can be used to estimate the fluid levels in a patient non-invasively. These measurements have been shown to be predictive of

heart failure decompensation up to 14 days before an event occurs. We have developed a portable bioimpedance system that can measure body impedance from 1 kHz to 1 MHz. The system uses the Magnitude-Ratio and Phase Difference Detection method to calculate the magnitude and phase of the measured impedance (see Figure 1). The system is enclosed in aluminum box (see Figure 2) and can be used with four co-axial cables. Each co-axial cable is actively driven by a screen driver circuit that reduces stray capacitance from the cables. Data from the device can be sent directly to a computer or transmitted over Bluetooth (with lid off). The device has been characterized with RC networks and will be validated in healthy volunteers.



▲ Figure 1: A schematic overview of the Magnitude-Ratio and Phase Difference Detection method. A fixed sinusoidal current is driven through the body and a sense resistance. The voltage is amplified and measured by a Gain-Phase Detector chip (AD8302).



▲ Figure 2: The portable bioimpedance spectroscopy measurement system inside the enclosure.

FURTHER READING

- M. Delano and C. Sodini, "A Long Term Wearable Electrocardiogram Measurement System," in Body Sensor Networks Conference, 2013 pp. 1-6.
- E. Winokur, M. Delano, and C. Sodini, "A wearable cardiac monitor for long-term data acquisition and analysis," IEEE Transactions on Biomedical Engineering, vol. 60, pp. 189-92, 2013.
- E. Winokur, D. He, and C. Sodini, "A wearable vital signs monitor at the ear for continuous heart rate and pulse transit time measurements," in IEEE EMBC, 2012 pp. 2724-7.

A Subdermal EEG Monitor for Seizure Detection

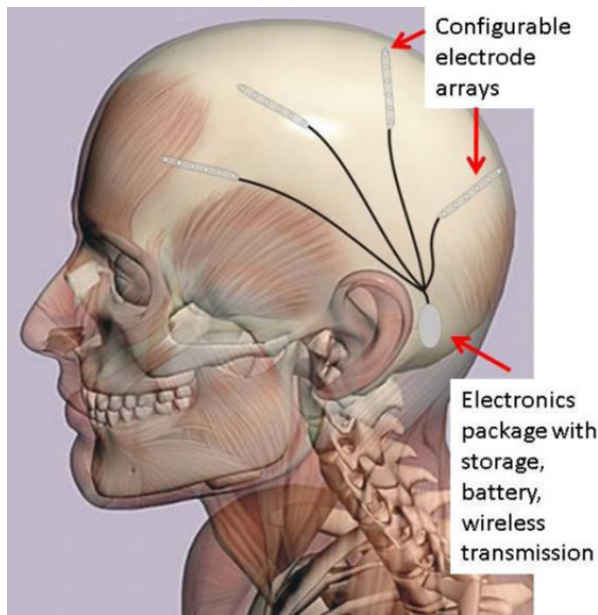
B. Do Valle, C.G. Sodini

Sponsorship: Center for Integrated Circuits and Systems

Epilepsy is a common chronic neurological disorder that affects about 1% of the world population. It is characterized by repeated seizures, which are caused by an abnormal neuronal firing in the affected brain area. Although EEG has been the chief modality in the diagnosis and treatment of epileptic disorders for more than half a century, long-term recordings (days to weeks) can be obtained only in the hospital setting. Many patients, however, have intermittent seizures occurring far less often. Patients cannot come into the hospital for weeks on end for an event to be captured on EEG – a necessary prerequisite for making a definitive diagnosis, tailoring therapy, moving toward certain kinds of solutions such as surgery, or even establishing the true rate of events. This work aims to address this need by proposing a subdermal implantable 8-channel

EEG monitor and seizure detector. The system will be implanted behind the patient's ear, as shown in Figure 1, to guarantee continuous monitoring of the brain's activity. The first step towards creating the implantable EEG monitor was to understand the challenges in recording EEG. To do that, we designed a behind-the-ear-wearable device using off-the-shelf components that is currently being tested at MGH.

The wearable prototype consists of 1 EEG channel sampled at 256 Hz with a 12-bit resolution. The system is housed in a package, shown in Figure 2, created by a 3D printer. One electrode is placed near the temporal lobe (close to T3 or T4), and the other one is placed on the mastoid. The data is transmitted through Bluetooth Low Energy to an iPod Touch, which uploads the data to a secure server via WiFi.



▲ Figure 1: Implanted EEG system showing the location of the electronic package and electrodes.



▲ Figure 2: Behind-the-ear wearable prototype currently being tested at MGH.

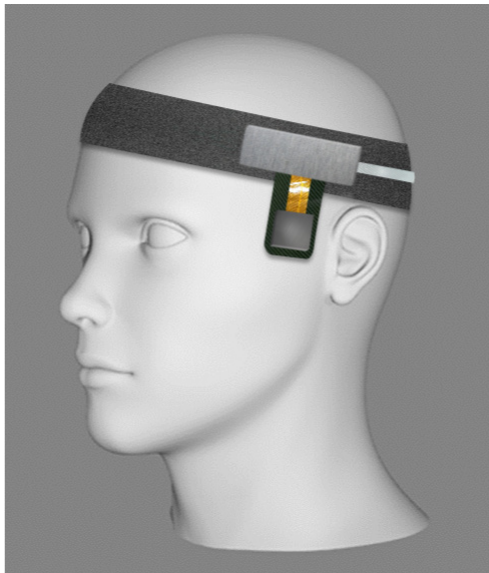
An Electronically Steered, Wearable Transcranial Doppler Ultrasound System

S. Pietrangelo, C.G. Sodini, H.-S. Lee
Sponsorship: Medical Electronic Device Realization Center

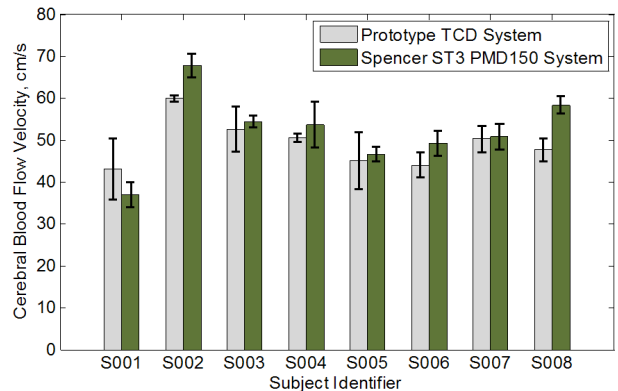
The central objective of critical care for patients affected by neurotrauma, cerebrovascular accident (i.e., stroke), and other neurovascular pathologies is to monitor the patient's state and provide suitable medical intervention to mitigate secondary injury and aid in recovery. While several non-invasive cerebrovascular diagnostic modalities exist, the use of transcranial Doppler (TCD) sonography is highly compelling for certain diagnostic needs due to its safety in prolonged studies, high temporal resolution, and relative portability. Despite a growing list of potential diagnostic applications, several constraints – notably operator-dependent measure-

ment results and the need for manual vessel location – have generally confined the use of TCD ultrasound to highly specific clinical environments (e.g., neurocritical care units and vascular laboratories).

Figure 1 illustrates a conceptual TCD system for wearable, autonomous monitoring of cerebrovascular state. Figure 2 compares clinically measured cerebral blood flow velocity data from a first-generation TCD prototype system to a commercially available TCD system. Comparable velocimetry data was obtained using both systems across several different human test subjects.



▲ Figure 1: Concept of a wearable TCD monitoring system with integrated ultrasound electronics.



▲ Figure 2: Comparison of average cerebral blood flow velocity across subject trials.

FURTHER READING

- S. J. Pietrangelo, "An electronically steered, wearable transcranial Doppler ultrasound system," Master's thesis, Massachusetts Institute of Technology, Cambridge, 2013.

Continuous and Non-invasive Blood Pressure Monitoring using Ultrasonic Methods

J. Seo, H.-S. Lee, C.G. Sodini

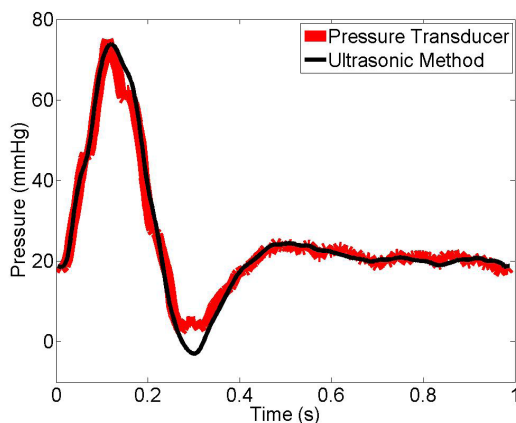
Sponsorship: Samsung Fellowship, Center for Integrated Circuits and Systems

An arterial blood pressure (ABP) waveform provides valuable information in treating cardiovascular diseases. The ABP waveform is usually obtained through a pressure transducer connected to an arterial catheter. Although considered as the gold standard, the disadvantage of this method is its invasive nature. The invasive nature not only increases various patients' risks but makes the usage of the ABP waveform for cardiovascular studies expensive. Therefore, reliable non-invasive ABP waveform estimation has been desired for a long time by medical communities. In that sense, medical ultrasound is an attractive imaging modality because it is inexpensive, free of radiation, cuff-less and suitable for portable system implementation.

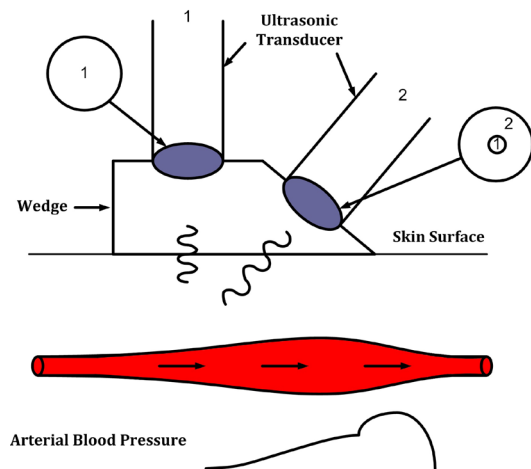
The proposed ultrasonic ABP monitoring is achieved by observing the pulsatile change of the cross-sectional area and identifying the elastic property of an arterial vessel, represented by the pulse wave velocity (PWV; the

propagation speed of a pressure wave along an arterial tree) with a diastolic blood pressure measurement as a baseline. The PWV can be estimated by obtaining a flow-area plot and then measuring the slope of a linear part in the flow-area plot during a reflection-free period (e.g., the early systolic stage).

An experimental setup was established to validate this pressure estimation technique. The cross-sectional area is estimated from the ultrasonically obtained diameter waveform assuming axisymmetric geometry of a tube. The volumetric flow rate is calculated from the spatial mean velocity of scatterers inside the tube using Doppler ultrasound. Figure 1 compares the resulting pressure waveform from ultrasonic methods to the waveform from a pressure transducer, which shows an excellent agreement. Figure 2 shows a prospective schematic of ultrasonic transducers for a clinical test.



▲ Figure 1: Comparison of two pressure waveforms. Assuming the mean pressure of two waveforms are same, a pressure waveform obtained from ultrasonic methods well agrees with a direct pressure waveform measurement from a pressure transducer.



▲ Figure 2: Prospective schematic of ultrasonic transducers for a clinical test. Channel 1 measures a vessel diameter while channel 2 measures a blood flow velocity simultaneously to estimate a local PWV and an ABP waveform.

FURTHER READING

- B. W. A. M. M. Beulen, N. Bijnens, G. G. Koutsouridis, P. J. Brands, M. C. M. Rutten and F. N. Van De Vosse "Toward noninvasive blood pressure assessment in arteries by using ultrasound," *Ultrasound in Medicine and Biology*, vol. 37, no. 5, pp. 788-797, 2011.
- S. I. Rabben, N. Stergiopoulos, L. R. Hellevik, O. A. Smiseth, S. Slordahl, S. Urheim and B. Angelsen "An ultrasound-based method for determining pulse wave velocity in superficial arteries" *Journal of Biomechanics*, vol. 37, pp. 1615-1622, 2004.

Body-coupled Communication and Implants

G.S. Anderson, C.G. Sodini

Sponsorship: Center for Integrated Circuits and Systems

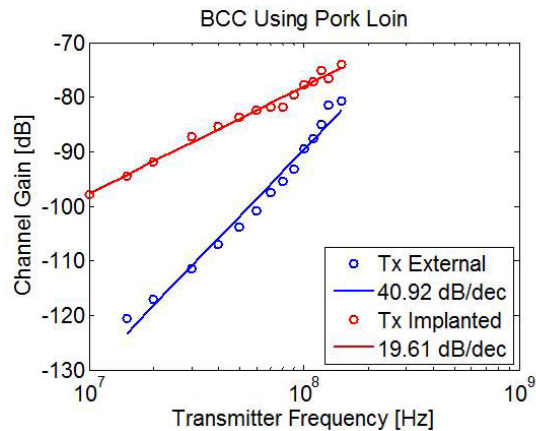
Body-coupled communication (BCC) is achieved by creating a potential difference in one area of the body and sensing the resulting attenuated potential difference in another area of the body. To do this, the transmitter and receiver each have two electrodes that electrically connect to the body's conductive tissues beneath the epidermis. These connections can be formed either capacitively or galvanically. A capacitive link consists of the electrode forming one plate of a parallel plate capacitor while the conductive tissues form the other plate. A galvanic link is formed by directly putting the electrode/wire in the conductive tissue.

For an implant to communicate to a device outside the body using BCC, the channel utilizes both galvanic and capacitive links (capacitive for the device outside the body and galvanic for the implant). To test if this is

possible a pork loin was used to simulate the conductive tissue of the body (see Figure 1). First, both the transmitter's and receiver's electrodes were connected to the pork loin using cardboard spacers between the pork loin and the electrodes, ensuring that both the transmitter and receiver would be capacitively coupled to the conductive tissue in the pork loin. Next the transmitter's output was connected to two alligator clips that were inserted into the pork-loin while the receiver was connected capacitively as before. This configuration simulates an implanted transmitter that is galvanically coupled to the conductive tissue, communicating with a receiver that is capacitively coupled. The results, shown in Figure 2, validate the predictions of the body model detailed in the further reading below



▲ Figure 1: A setup to test implants talking to devices outside the body using BCC.



▲ Figure 2: BCC channel measurements.

FURTHER READING

- G. S. Anderson and C. G. Sodini, "Body coupled communication: The channel and implantable sensors," Body Sensor Networks (BSN), 2013 IEEE International Conference on , vol., no., pp. 1.5, 6-9 May 2013.
- T. G. Zimmerman, "Personal Area Networks (PAN): Near-field intrabody communication," Master's thesis, Massachusetts Institute of Technology, Cambridge, 1995.
- A. Fazzi et al., "A 2.75mW wideband correlation-based transceiver for body-coupled communication," ISSCC Dig. Tech. Papers, pp. 204-205, Feb. 2009.

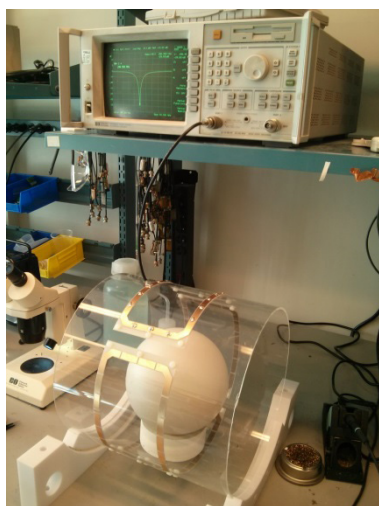
Automated Design of a Robust Decoupling Matrix for Multi-channel Parallel Transmit Coil Arrays in Magnetic Resonance Imaging

Z. Mahmood, B. Guérin, B. Keil, E. Adalsteinsson, L.L. Wald, L. Daniel
Sponsorship: NIH, NSF NCN – NEEDS Node, SRC

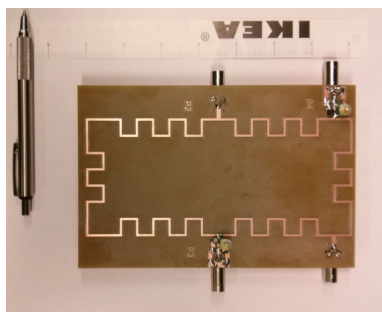
In a coupled parallel transmit array, the power delivered to a channel is partially distributed to other channels because of coupling. This power is dissipated in the circulators, resulting in a significant reduction in the power efficiency of the overall system. Most existing decoupling methods focus on nearest-neighbor channels. Capacitive ladder networks, which aim at decoupling also distant neighbors, are highly sensitive to specific operating conditions; they are rarely used because of this lack of robustness. In this work, we propose an automated approach to design a robust decoupling matrix interfaced between the RF amplifiers and the coils. Similar to a Butler matrix, our decoupling matrix mixes the input signals but is also optimized to ensure that all forward power is delivered to the load. In addition to mixing the input signals to provide uncoupled field patterns, the decoupling matrix also minimizes the power lost in the circulators.

The decoupling condition is that the impedance matrix seen by the power amplifiers is a diagonal matrix

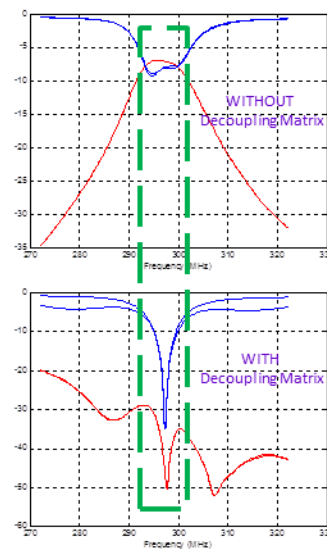
with 50 ohms at the diagonal. Intuitively, a dense full rank matrix can be converted to a diagonal matrix by eigen-decomposition. In this work, we diagonalize the impedance matrix of the coupled coils (or antennas) by a multiplication with its eigen-vectors. We accomplish this multiplication via Givens rotations implemented using only passive RF components such as hybrid couplers and lumped reactive elements, as shown in Figure 2. We explore several design aspects of the decoupling matrix, including the network topology, robustness and sensitivity to component values by designing a decoupling matrix for a 2-channel coupled array for magnetic resonance imaging. The results, shown in Figure 3, show that our decoupling matrix achieves near-ideal decoupling. The 2-channel instantiation works for demonstration and evaluation purposes to illustrate the principles of robustness and topology exploration. The methods presented in this abstract scale to any arbitrary number of channels and can be readily applied to other coupled systems such as antenna arrays.



▲ Figure 1: Picture of a coupled 7-Tesla parallel transmit head array to be decoupled.



▲ Figure 2: Layout of a decoupling matrix designed to decouple 2-channels.



▲ Figure 3: Measured S-parameters of a 2-channel array without (top) and with (bottom) a decoupling matrix.

FURTHER READING

- Z. Mahmood, B. Guérin, E. Adalsteinsson, L. Wald, and L. Daniel, "An Automated Framework to Decouple pTx Arrays with Many Channels," in *Proc. 21st Annual Meeting & Exhibition of International Society for Magnetic Resonance in Medicine (ISMRM)*, Apr. 2013.
- Z. Mahmood, B. Guérin, B. Keil, E. Adalsteinsson, L. L. Wald, and L. Daniel. "Design of a Robust Decoupling Matrix for High Field Parallel Transmit Arrays" in *Proc. 22nd Annual Meeting & Exhibition of International Society for Magnetic Resonance in Medicine (ISMRM)*, May, 2014.

Ultimate Performance Metrics for Magnetic Resonance Imaging RF Coil Designs

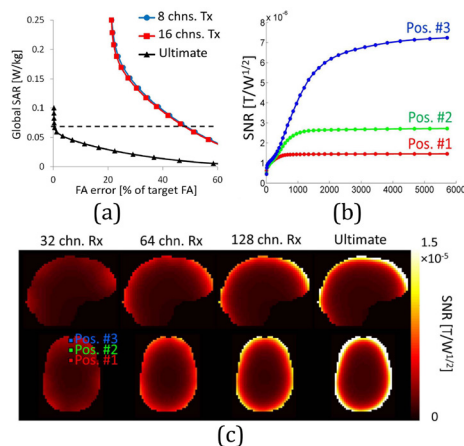
J. Fernández Villena, A.G. Polimeridis, B. Guerin, L.L. Wald, E. Adalsteinsson, J.K. White, L. Daniel.
Sponsorship: NIH, MIT Skoltech Initiative

High and ultra-high field (3T, 7T, and beyond) MRI scanners allow improving the signal-to-noise ratio (SNR) and thus image quality. Increasing the frequency (and reducing the wavelength) leads to undesired effects, such as non-uniformity of the magnetic field components within the body, which is ultimately translated into loss of image contrast. Parallel MRI and parallel transmission techniques, using multiple receiving (Rx) and transmitting (Tx) channels, have been introduced to address some of these issues. However, in addition to the higher energy deposition in the body due to the increased field, the use of multiple excitation channels can lead to undesired effects that may increase the local power deposition in certain body areas. To comply with safety limits, the specific absorption rate (SAR), i.e., the rate at which energy is absorbed by the body when exposed to an electromagnetic (EM) field, must be locally monitored and limited. Based on constrained optimization and using the EM field distribution generated by each channel of a given coil array, the RF excitation pulses can be controlled to maximize SNR while minimizing the SAR.

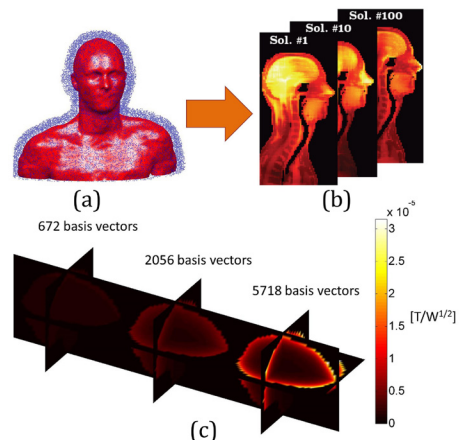
The ultimate SNR and SAR are the best values that such optimization could achieve for any possible coil design. Their computation requires a complete basis for the EM fields in the sample under study, i.e., the body.

Existing methods are based on analytical solutions, which only allow the computation of the ultimate SNR and SAR for simple homogeneous spheres and cylinders. Despite the insight gained from these metrics, MRI RF coils are intended for realistic body models. Therefore, results for highly complex inhomogeneous realistic body models can give extremely useful information, insight and intuition to coil designers, and define ultimate figures of merit against which to benchmark new prototype designs (Figure 1).

In collaboration with the RLE MRI group and the HST/MGH A. A. Martinos Center for Biomedical Imaging, we have developed a methodology for generating the basis for the EM fields that any coil design can induce in realistic human body models. The generation of this basis (illustrated in Figure 2) involves the combination of the integral equation formulation of the Maxwell equations, the concepts of the Huygens equivalence surface principle, the application of randomized singular value decomposition (SVD) approaches for the generation of a basis of extremely large operators, and the development of very fast volume integral equation solvers. This basis can be used to generate the ultimate SNR and SAR in realistic body models.



▲ Figure 1: (a) SAR versus flip angle curves, for 8 and 16 channels Tx arrays, and the ultimate solution. (b) Convergence of the SNR to the ultimate value with increasing number of vectors for 3 different brain positions. (c) SNR maps for 32, 64 and 128 channels Rx coil arrays, and ultimate values.



▲ Figure 2: (a) From body model and Huygens surface to (b) EM basis vectors. (c) Evolution of the SNR brain maps with increasing number of vectors.

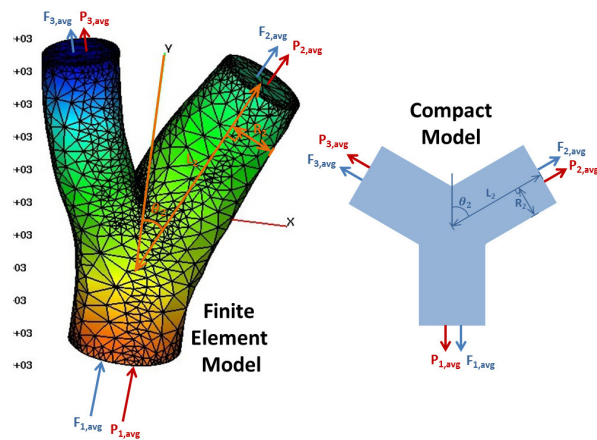
FURTHER READING

- B. Guerin, J. Fernández Villena, A. G. Polimeridis, E. Adalsteinsson, L. Daniel, J. K. White, and L. L. Wald, "The ultimate SNR and SAR in realistic body models," ISMRM 2014 Annual Meeting, May 2014.
- A. G. Polimeridis, J. Fernández Villena, L. Daniel and J. K. White, "Stable FFT-JVIE Solvers for Fast Analysis of Highly Inhomogeneous Dielectric Objects," Journal of Computational Physics, vol. 269, pp. 280-296, 2014.

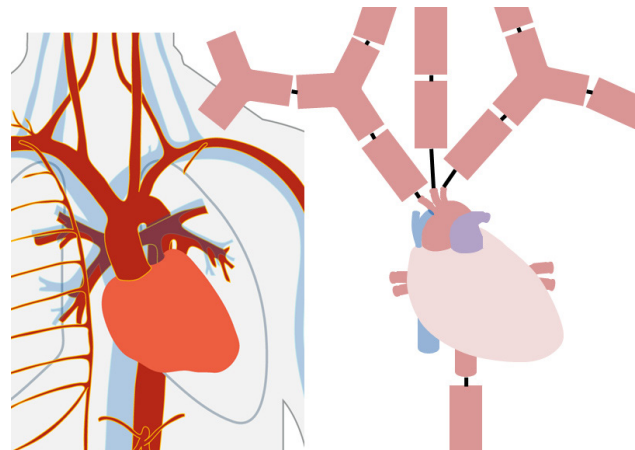
Compact Dynamic Modeling for Large-Scale Cardiovascular System Simulation

Y.-C. Hsiao, Y. Vassilevski, S. Simakov, L. Daniel
Sponsorship: MIT Skoltech Initiative

Diagnosing medical conditions based on non-invasive (or minimally invasive) measurements requires simultaneous modeling of both (1) local arteries in pathological states, and (2) global large-scale arterial networks from which pressure and flow are directly accessible. For instance, diagnosing atherosclerosis or an aneurysm requires the detailed pressure and flow inside local arterial bifurcation segments as for (1). Such fluid-mechanical interaction problems are solvable by finite-element methods (Figure 1). The simulated pressure and flow are compared against measurements to ensure model quality. However, because of the limited measurability of pressure and flow at pathological sites, it is crucial to develop accurate yet computationally tractable models for global arterial networks to correlate the pathological conditions with the measurements taken from larger vessels in global networks. The final diagnosis can be obtained by solving an inverse problem for the pathological parameters, for instance, aneurysm internal diameter, arterial wall thickness, plaque stiffness, etc.



▲ Figure 1: Left: Pressure profile of a bifurcation solved by finite element methods. The length of each branch is chosen such that Poiseuille flow is fully developed to satisfy network port assumptions. Right: Compact model generated by our algorithms.



▲ Figure 2: Left: Physiological arterial network. Right: Arterial network model that consists of a heart model and local dynamic models of straight and bifurcation arteries.

FURTHER READING

- B. Bond, T. Moselhy, and L. Daniel, "System identification techniques for modeling of the human arterial system," in Proc. SIAM Conference on the Life sciences, Pittsburgh, PA, July 2010, p. 12-15.
- Y.-C. Hsiao, L. Daniel, "Sparse basis pursuit on automatic nonlinear circuit modeling," presented at IEEE International Conference on ASIC (ASICON), Shenzhen, China, 2013

Towards Wireless Capsule Endoscopic Ultrasound (WCEU)

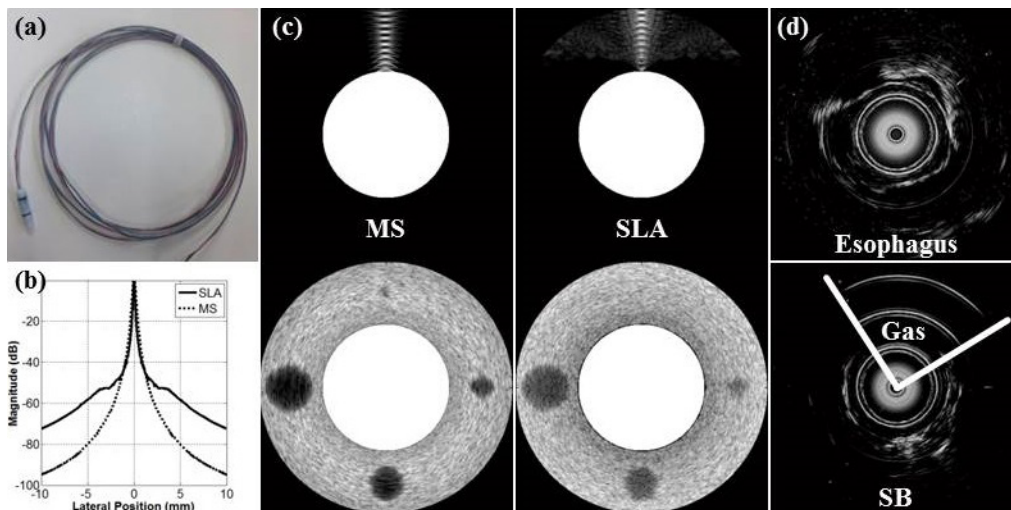
J.H. Lee, C.M. Schoellhammer, G. Traverso, D. Blankschtein, R. Langer, K.E. Thomenius, B. Anthony, D.S. Boning

Imaging of the small bowel (SB) is challenging due to its length and winding path. Wireless Capsule Endoscopy (WCE) provides convenient access to the SB but lacks ultrasound imaging capabilities necessary for accurate diagnosis. Wireless capsule endoscopic ultrasound (WCEU) combines the benefits of WCE and ultrasound imaging. This work evaluates transducer designs appropriate for WCEU in regard to image quality, system complexity, and cost and investigates whether the SB can produce sufficient contact to ensure acoustic coupling necessary for ultrasound imaging.

We evaluated mechanical-scanned (MS) and side-looking array (SLA). MS is implemented with a focused disc transducer and a motor; SLA uses TX and RX focusing with fixed F-numbers. Simulations of point and cyst phantoms were done using Field II. The MS tethered capsule developed for imaging feasibility study shown in Figure 1(a) consists of a 10 MHz transducer and a micro stepper motor with a 4 m long tether. *Ex vivo* pig tissue imaging was done to evaluate image quality. *In vivo* pig esophagus, stomach, and SB imaging were performed using the tethered capsule.

Simulation results are shown in Figures 1(b) and (c). MS performs better for both point and cyst imaging. SLA suffers in the near zone due to the small number of active elements and in the far zone due to large side lobes caused by the curvature of the capsule. Despite the motor, MS has a much simpler system than SLA, which requires a very large number of elements (> 400 for 10 mm ϕ at $\lambda/2$ spacing), multiplexing, parallel channel front-end and beamforming. MS power can suffer due to the motor, but SLA power suffers from a significantly more complex signal chain. With current transducer technology, the cost for SLA is prohibitively high to be a disposable device.

Figure 1(d) shows *in vivo* images. Full circumferential coverage was difficult to maintain due to partial contact with the capsule. Peristalsis can potentially produce better coupling, but its effect could not be adequately examined due to reduced activity under anesthesia. With current technology, MS shows better performance overall. *In vivo* imaging shows promising results although the effects of peristalsis and resulting coverage need to be further investigated.



▲ Figure 1: (a) Tethered capsule for experiment. (b) Beam profile comparison for SLA and MS. (c) Simulation of point and cyst imaging for MS and SLA. (d) Ultrasound image of esophagus and SB from pig *in vivo* experiment.

FURTHER READING

- J. L. Toennies, G. Tortora, M. Simi, P. Valdastrri, and R. J. Webster, "Swallowable medical devices for diagnosis and surgery: The state of the art," *Journal of Mechanical Engineering Science*, vol. 224, no. 7, pp. 1397-1414, July 2010.

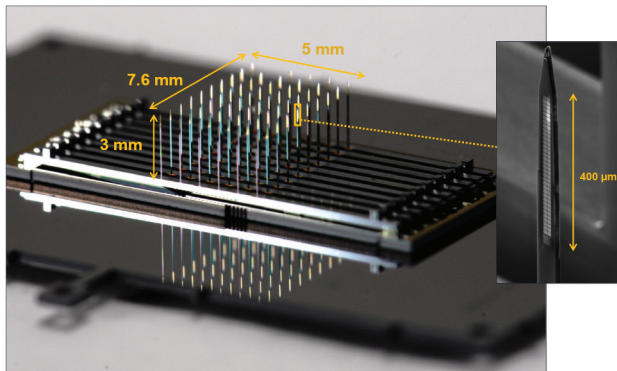
High-Density, Three-Dimensional Microelectrode Arrays for Neural Recording

J. Scholvin, A.N. Zorzos, C.G. Fonstad Jr., E.S. Boyden
Sponsorship: Simons Center for the Social Brain, Allen Institute, NIH

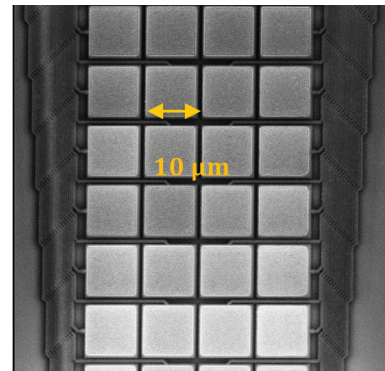
Our research focuses on strategies for designing and fabricating three-dimensional microelectrode arrays, to be used for extracellular neural recording. Our designs have customizable electrode locations, targetable to specific neural substrates, and distributed in a volume throughout a neural network in the mammalian brain. We accomplish this by utilizing MEMS microfabrication techniques to create a number of planar structures that are mechanically and electrically assembled into a three-dimensional array (Figure 1). The resulting array consists of a large number of thin needles, and each needle contains many recording sites along its length. To pick up neural activity, exposed metal recording sites are located in along the length of each of the needles (Figure 2). These record-

ing sites are routed along the needle and aggregated at the base of the array, for further routing, amplification and digitization off-chip.

Our approach relies on a number of innovations in different parts of the system design. We developed a simple and customizable toolset to automatically generate the different design components needed, which we then fabricate and assemble into a three-dimensional array. Further, we created mechanical and electrical connections for the arrays as well as packaging solutions aimed at head-fixed recordings in rodents. Finally, we are using electron beam lithography to define sub-micron pitched long metal lines for signal routing, which allows us to create very narrow needles that minimize tissue displacement.



▲ Figure 1: Photograph showing a 4080 channel 3-D probe, consisting of 6x10 needles. Each needle, as shown in the insert, contains 68 high-density recording sites on its surface, arranged as two columns of 34 sites each.



▲ Figure 2: Electron micrograph of the high-density recording site configuration, for a four column configuration. Each recording site is approximately 10 μm in size, and densely packed so that the activity of a neuron is picked up by multiple sites simultaneously, enabling automated data analysis.

FURTHER READING

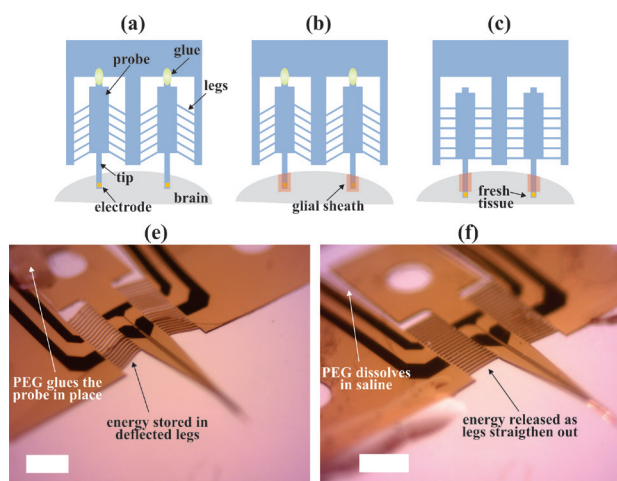
- J. Scholvin, S. K. Arfin, J. Bernstein, J. Kinney, C. Moore-Kochlacs, A. N. Zorzos, N. Kopell, C. G. Fonstad, E. S. Boyden, 10/16/2012, "Scalable 3-d microelectrode recording architectures for characterization of optogenetically modulated neural dynamics", Society for Neuroscience, Annual Meeting, New Orleans LA, 2012
- J. P. Kinney, C. Wentz, S. Arfin, J. Bernstein, J. Scholvin, C. Moore-Kochlacs, N. Kopell, E. Boyden, 10/16/2012, "Hardware and software architectures for supporting scalable electrophysiological signal amplification, acquisition, storage, and analysis", Society for Neuroscience, Annual Meeting, New Orleans LA, 2012
- C. Moore-Kochlacs, J. P. Kinney, J. G. Bernstein, S. K. Arfin, J. Scholvin, N. Kopell, E. S. Boyden, 10/14/2012, "Spike sorting for spatially dense high channel count extracellular recordings", Society for Neuroscience, Annual Meeting, New Orleans LA, 2012

Reconfigurable Neural Probes for Chronic Electrical Recording

A. Dighe, U. Froriep, M. Sunshine, A. Ievins, P. Anikeeva, C. Moritz, J. Voldman
Sponsorship: National Science Foundation Center for Sensorimotor Neural Engineering (CSNE)

Chronic interfaces with the nervous system are critical for understanding basic neurobiology as well as for enabling new technologies that could be used in neurorehabilitation and in the treatment of various neurological disorders. A major challenge with current brain-computer interfaces is their inability to reliably record single-unit electrical activity over long periods of time (months) due to tissue reaction to foreign objects in the brain. This tissue reaction consists of a sheath of glial cells that encapsulates a neural probe a few weeks after implantation. Here we describe the design of a new neural probe that aims to bypass the body's immune reaction by changing shape once implanted in the brain, thereby providing the ability to chronically monitor neural activity *in vivo*.

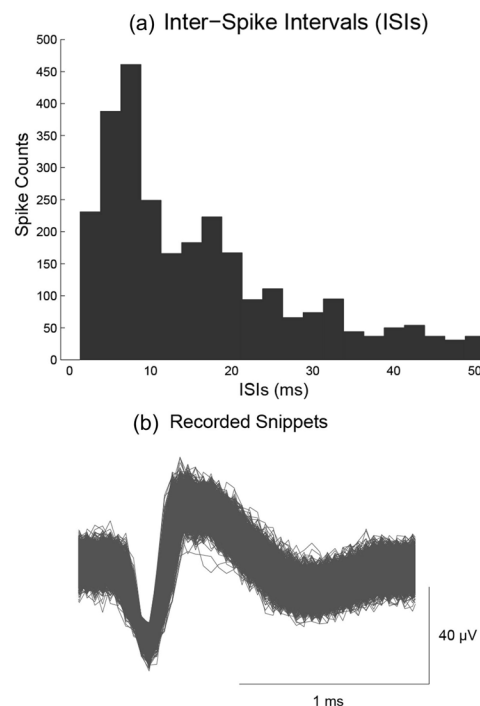
Our reconfigurable electrode consists of a thin polymer probe whose body can be deflected and locked prior to insertion via a dissolvable glue such as polyethylene glycol (PEG), storing mechanical energy in the device legs (Figure 1a). After inserting into the brain and waiting for the initial glial sheath to form (Figure 1b), the device can be triggered by dissolving the glue, causing the recording tip of the device to penetrate into fresh tissue (Figure 1c). Designing the tip dimensions to be small (7-20 μm) should prevent the formation of an additional glial sheath post-triggering. We have demonstrated successful triggering and electrical recordings from this device in an acute setting in the rodent brain (Figure 2). This technology holds promise for creating chronic interfaces for recording stable neural activity.



▲ Figure 1: (a) Schematic showing probe deflected and glued prior to insertion into brain. (b) A glial sheath forms over time (~weeks). (c) Dissolving the glue triggers the probe body, pushing it into fresh tissue. (e, f) Photographs of device before and after deployment. Scale bars = 500 μm .

FURTHER READING

- A. Dighe, U. Froriep, M. Sunshine, A. Ievins, P. Anikeeva, C. Moritz, and J. Voldman, "Development and *in vivo* testing of reconfigurable neural probes for chronic electrical recording," in *Solid-State Sensors, Actuators and Microsystems (Hilton Head) Workshop*, 2014, pp. 5-8.
- V. S. Polikov, P. A. Tresco, and W. M. Reichert, "Response of brain tissue to chronically implanted neural electrodes," *Journal of Neuroscience Methods*, vol. 184, pp. 1-18, Oct. 2005.
- T. D. Y. Kozai, N. B. Langhals, P. R. Patel, X. Deng, H. Zhang, K. L. Smith, J. Lahann, N. A. Kotov, and D. R. Kipke, "Ultrascale implantable composite microelectrodes with bioactive surfaces for chronic neural interfaces," *Nature Materials*, vol. 11, no. 12, pp. 1065-1073, Dec. 2012.



▲ Figure 2: Inter-spike interval (ISI) histogram (top) and time-amplitude sorted waveforms (bottom) recorded intra-operatively immediately following device insertion in a rodent motor cortex.

Thermal Drawing of Minimally Invasive Neural Probes

A. Canales, C. Tringides, U.P. Froriep, Y. Fink, P.O. Anikeeva

Sponsorship: National Science Foundation, McGovern Institute for Brain Research, Simons Center for the Social Brain

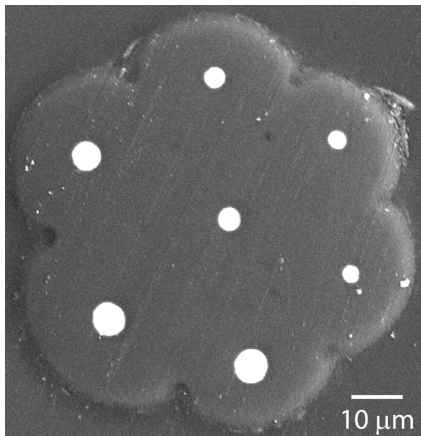
Understanding the mechanism of debilitating neurological conditions and to enable treatment of these conditions requires reliable recordings of neural activity. Currently available neural probes, however, are limited by deterioration of the electrode-tissue interface supposedly caused by glial scarring and neuronal death around the probe.

It has been hypothesized that the two main characteristics of neural probes leading to scarring and inflammatory tissue response are the size and the mechanical flexibility of the probe. Thus, flexible, minimally invasive neural probes could be invisible to the neural tissue, and thus could help to decrease tissue response to the device.

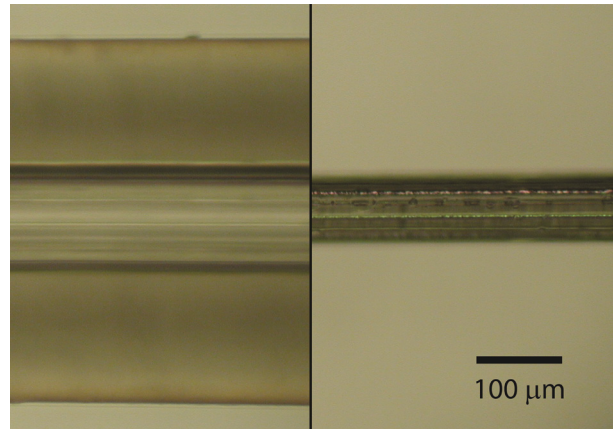
To fabricate this kind of probes we apply a thermal drawing process. To this end we start with a template (~2.5-4 cm in diameter), and apply controlled

heat and stress to obtain hundreds of meter long fiber with preserved cross-sectional geometry, but reduced in diameter to the micrometer scale. This way, the recording surface of the electrodes can be tuned down to $<1 \mu\text{m}$, while maintaining controlled pitch.

To achieve a device with low bending stiffness, making it a promising candidate for minimally invasive recordings in neural tissue, we insulated electrodes using two polymer types. In addition, different chemical properties of these two polymers make it possible to employ chemical etching to further modify the geometry of the fiber. The latter allows us to reduce the size of the probe that incorporates 7-10 electrodes to an overall diameter $<100 \mu\text{m}$. Our *in vivo* studies show that the fiber probes record neural activity with a signal-to-noise ratio of up to 20.



▲ Figure 1: Cross-section of the neural probe. metal electrodes (white) are cladded by a polymer that provides electrical insulation and mechanical support.



▲ Figure 2: Comparison of the fiber before (left) and after (right) etching the polymer cladding. This process increases the mechanical flexibility and decreases the size of the probes.

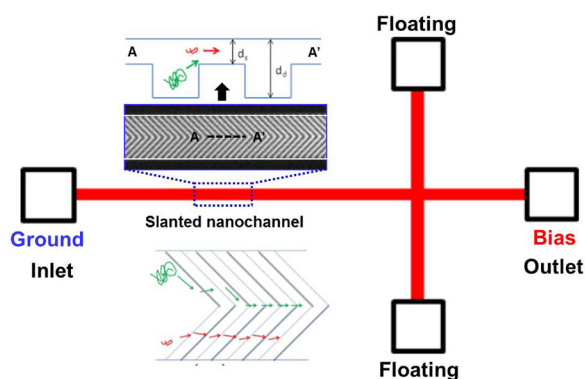
Size-based Biomolecule Preconcentration using Herringbone Nanofilter Arrays

S.H. Ko, J. Han
Sponsorship: DARPA

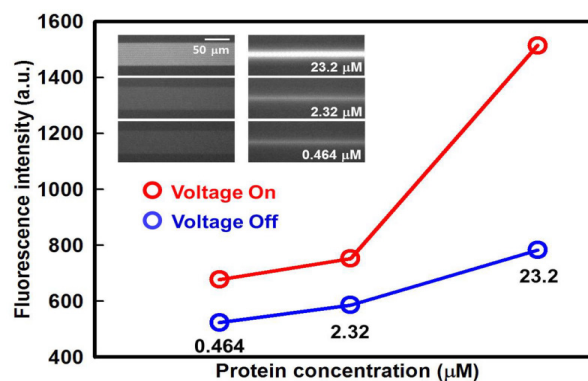
Micro- and nanofluidic-base sample analysis chips (e.g., labs-on-a-chip) have many advantages over traditional benchtop analyzers, but they suffer from poor detection efficiency because of small sample volume and low optical path length. As a result, many research groups have developed and demonstrated high-performance detection tools (enhancing detection sensitivity) and sample preconcentration methods (directly enhancing signal). Of these, our group has focused on developing mobility-base preconcentrators (charge to size ratio). We recently designed a new size-based biomolecule preconcentrator. This device consists of herringbone nanofilter arrays (HNAs) with periodically patterned deep and shallow nanoslits, as in Figure 1. By the Ogston sieving theory, while small molecules are more likely to flow across in a straight line, large ones are more likely to move toward the center of HNAs, so that relatively large molecules, compared to shallow nanoslit dimensions, can be focused on the center of the device. We demonstrated the preconcentration using trypsin inhibitor (21

kDa), which is denatured by SDS surfactant and heat, and labeled by non-covalent dye, as in Figure 2. In this device, the preconcentration factor and limit of detection (LOD) are about 7 times and 2.32 μM , respectively.

In general, size-based separation methods using nanofilter arrays have diffusion and dispersion issues in the downstream and low optical path length, which lead to a low detection signal. Since the operating mechanism of the HNA is consistent with that of existing nanofilter-base biomolecule separation devices, it is easier to integrate the HNA with the separation device than the mobility-base preconcentrator through standard fabrication. This method enables simultaneous preconcentration and separation of biomolecules in a single chip with operational simplicity, robustness, and minimal sample use. In addition, the HNA makes biomolecules with different sizes have their distinct trajectories and different extents of preconcentration factor, which results in an efficient continuous flow immunoassay.



▲ Figure 1: Schematic of HNAs with periodically patterned deep (120 nm) and shallow (60 nm) nanochannels. Driving force is electrophoresis (inlet-ground, out-positive bias).



▲ Figure 2: Demonstration of denatured trypsin inhibitor preconcentration. Red circles represent preconcentrated proteins, and blue ones are non-preconcentrated proteins. Inset images are fluorescence images before (left) and after (right) preconcentration.

FURTHER READING

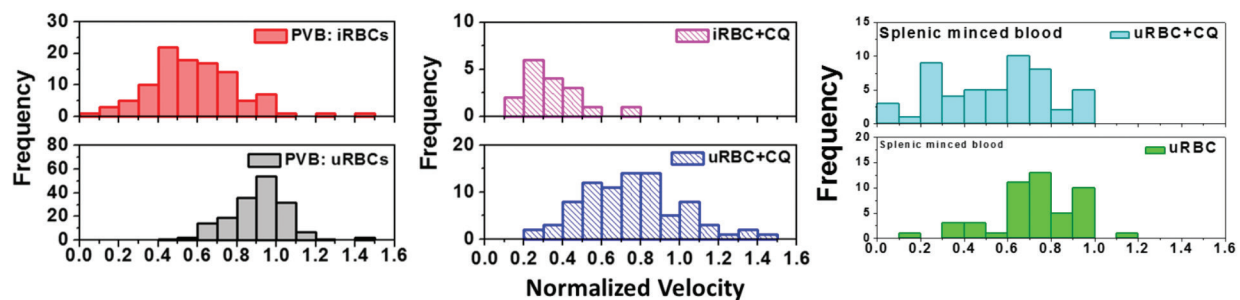
- A. G. Ogston, "The spaces in a uniform random suspension of fibers," *Transactions of the Faraday Society*, vol. 54, pp. 1754-1757, 1958.
- L. F. Cheow, H. Bow, and J. Han, "Continuous-flow biomolecule concentration and detection in a slanted nanofilter array," *Lab on a Chip*, vol. 12, pp. 4441-4448, 2012.
- J. Fu, R. B. Schoch, A. L. Stevens, S. R. Tannenbaum, and J. Han, "A patterned anisotropic nanofluidic sieving structure for continuous-flow separation of DNA and proteins," *Nature Nanotechnology*, vol. 2, pp. 121-128, 2007.

Red Blood Cell Deformability and Splenic Clearance in *Plasmodium yoelii* Infected Mice

S. Huang, A. Amaladoss, M. Liu, H. Chen, R. Zhang, P. Preiser, M. Dao, J. Han
Sponsorship: SMART

During *Plasmodium yoelii* infection, the mechanical filtration of red blood cells in spleen plays an important role in the host's defense against malaria parasites (1). Small changes in RBC deformability may significantly impact on the pathophysiological outcome (2). In this project, we attempted to gain a better understanding of malaria pathology through the mechanical reten-

tion of RBC in spleen. We independently studied the *in vitro* and *in vivo* impacts of malaria infection and/or drug treatment on RBC deformability(3, 4). With the microfluidic platform, the dynamic deformability of RBCs were quantitatively measured. Several important aspects pertaining to anemia and splenic retention were explored.



▲ Figure 1: uninfected and infected RBC deformability (velocity) from peripheral blood (left). The effect of antimalarial drug chloroquine drug treatment on peripheral blood deformability (middle) as well as on splenic blood deformability (right)

FURTHER READING:

- K. Chotivanich *et al.*, Central Role of the Spleen in Malaria Parasite Clearance. *Journal of Infectious Diseases* **185**, 1538 (May 15, 2002, 2002).
- G. Deplaine *et al.*, The sensing of poorly deformable red blood cells by the human spleen can be mimicked in vitro. *Blood* **117**, e88 (February 24, 2011).
- S. Huang *et al.*, Dynamic deformability of *Plasmodium falciparum*-infected erythrocytes exposed to artesunate in vitro. *Integrative Biology* **5**, 414 (2013).
- H. Bow *et al.*, A microfabricated deformability-based flow cytometer with application to malaria. *Lab on a Chip* **11**, 1065 (2011).

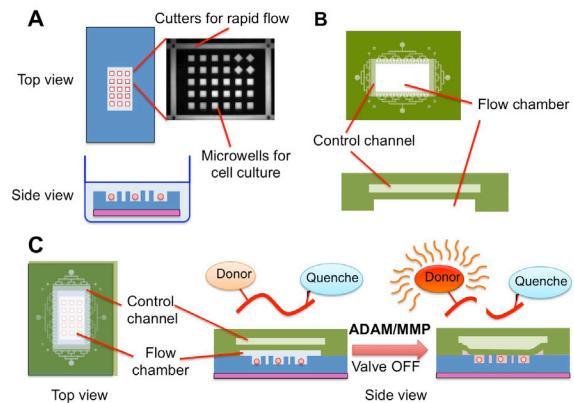
Microwell-based Platform For Single-cell Pericellular Protease Detection

L. Wu, J. Han

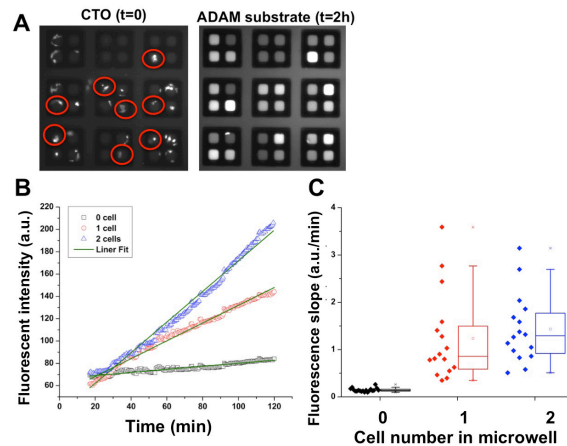
Sponsorship: Biosystems & Micromechanics IRG, SMART

Pericellular proteases, including those on cell surfaces and secreted ones, act as a key component of autocrine signaling and impact the microenvironment of individual cells. In particular, A disintegrin and metalloproteinases (ADAMs), which are typical kinds of pericellular protease expressed on cell surfaces, have been linked to various clinical pathological processes, including breast cancer progression. On one hand, previous studies suggest that the heterogeneous single-cell protease activity could lead to diverse cellular responses in terms of intracellular kinase activation profiles or cell migration patterns, emphasizing the need for single-cell study of pericellular protease response. On the other hand, no tool is available to measure the catalytic activity of those membrane-bound proteases directly at single cell level. In this work, we present a high-throughput microfluidic platform capable of monitoring single-cell pericellular protease activity.

The designed platform consists of two pieces (Figure 1). The bottom one has a microwell array pattern for cell culture; the top one includes a 2-layer structure for the valving function. Upon assembly of these two pieces by holding them together via mechanical clamping, one can pressurize the control layer of the assembled device to isolate individual microwells rapidly on demand. Thus the cell-surface protease activity measurement can be conducted by confining cells in individual microwells with diffusive FRET-based substrates. We tested the platform with HepG2 cells challenged with 1 μ M PMA, which is known as a strong stimulator for the shedding of several ADAM17 protease substrates. As shown in Figure 2, microwells of different cell numbers display fluorescent intensity profiles with diverse increasing rates, which are indicators for the protease activity level. These results confirm both the existence of heterogeneity in single-cell ADAM17 protease activity and the feasibility of our platform for studying the pericellular protease behavior of single cells.



▲ Figure 1: Schematic of microfluidic platform for single-cell protease activity measurement. Upon assembly (C) of bottom (A) & top pieces (B), the valve control layer allows pneumatic actuation of flow chamber ceiling to control the closing and opening of microwells.



▲ Figure 2: Heterogeneous protease response of HepG2 cells treated with 1 μ M PMA. (A) HepG2 cells stained with cell tracker orange (CTO) were confined in closed microwells with FRET-based substrate. Substrate fluorescence after 2h incubation is shown on right. (B) Representative fluorescent profile for microwells of different cell numbers. (C) Box plot of fluorescent slope for each microwell with 0, 1, or 2 cells.

FURTHER READING

- M. J. Duffy, E. McKiernan, N. O'Donovan, and P. M. McGowan, "The Role of ADAMs in Disease Pathophysiology." *Clinica Chimica Acta*, vol. 403, nos. 1-2, pp. 31-36, 2009.
- G. Maheshwari, H. S. Wiley, and D.A. Lauffenburger, "Autocrine Epidermal Growth Factor Signaling Stimulates Directionally Persistent Mammary Epithelial Cell Migration," *Journal of Cell Biology*, vol. 155, no. 7, pp. 1123-1128, 2001.
- K. Chalupsky, I. Kanchev, O. Zbodáková, H. Buryová, M. Jirousková, V. Korínek, M. Gregor, R. Sedláček, "ADAM10/17-Dependent Release of Soluble C-Met Correlates with Hepatocellular Damage," *Folia Biologica*, vol. 59, no. 2, pp. 76-86, 2013.

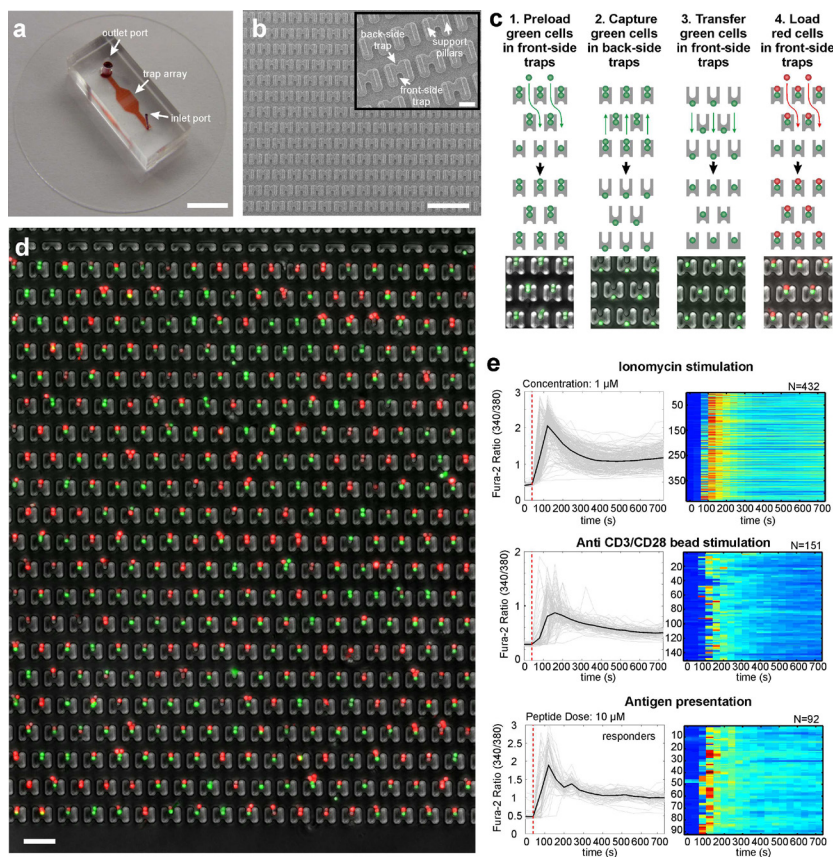
Cell Pairing for Studying Immunity

B. Dura, J. Voldman
Sponsorship: Singapore-MIT Alliance

Many immunological responses are mediated through direct cell-cell interactions. Engagement of immunoreceptors with their corresponding ligands initiates an intracellular signaling cascade that leads to a diverse array of responses including selection, differentiation, proliferation, and cytokine production. Our understanding of how immune responses are shaped by these interactions relies on our ability to examine direct dynamic interactions between immune cells and their partners. Methods to study these immune cell interactions, however, suffer from limited throughput and a lack of control over cell pairing. These limitations prevent statistical inference and complicate experimental analysis, thereby hindering their widespread use.

To address the major shortcomings of current approaches, we developed a microfluidic cell pairing

platform for studying immune cell interactions for numbers of cell pairs that afford meaningful statistical analysis (see Figure 1). The platform achieves cell pairing with accurate control in space and time with one-to-one interacting partners, well-defined and synchronous initiation of interaction, and enduring contacts. It enables the use of minimal numbers of primary immune cells ($\sim 10^4$ cells) and also allows control of the soluble microenvironment by exchange of media without losing cell registration. The pairing technique is compatible with pharmacological, antibody-based, and cellular modes of immune cell stimulation and enables us to examine the early interaction dynamics of immune cells in a highly controlled manner with quantitative analysis of their response profiles.



◀ Figure 1: Microfluidic device for immune cell pairing. (a) Image of device. (b) SEM image of cell trap array. (c) Four-step cell loading and pairing protocol. (d) Overlaid phase contrast and fluorescence images showing primary mouse lymphocytes stained with Dil (red) and DiO (green) membrane dyes paired in traps. (e) Ca^+ responses of OT-1 CD8 T cells with pharmacological (ionomycin), antibody-bead based (anti-CD3/28) and cell-based (SIINFEKL-loaded antigen presenting cells) stimulations. Scale bars: (a) 5 mm, (b) 100 μm , 20 μm (inset), (d) 50 μm .

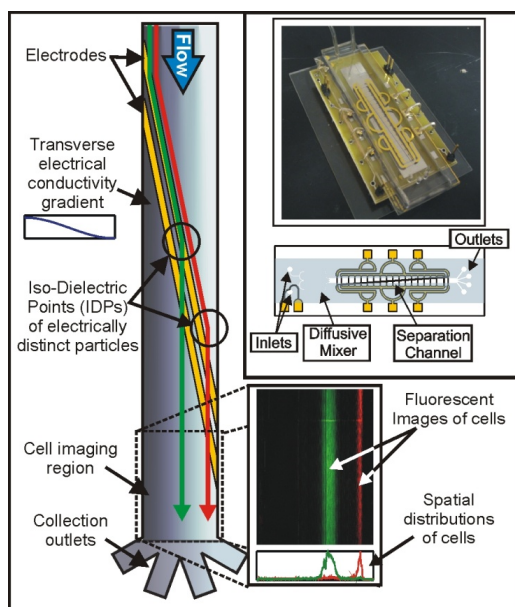
FURTHER READING

- A. M. Skelley, O. Kirak, H. Suh, R. Jaenisch, and J. Voldman, "Microfluidic Control of Cell Pairing and Fusion," *Nature Methods*, vol. 6, pp. 147-52, 2009.

Iso-dielectric Separation of Cells and Particles

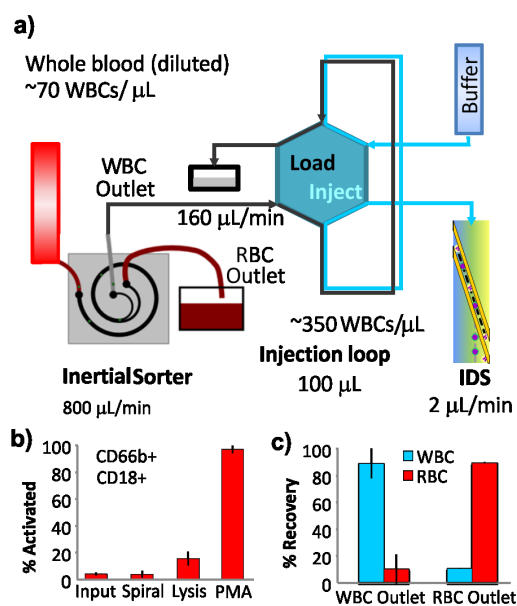
H.W. Su, J. Voldman
Sponsorship: DARPA

The development of new techniques to separate and characterize cells with high throughput has been essential to many of the advances in biology and biotechnology over the past few decades. We are developing a novel method for the simultaneous separation and characterization of cells based upon their electrical properties. This method, iso-dielectric separation (IDS), uses dielectrophoresis (the force on a polarizable object) and a medium with spatially varying conductivity to sort electrically distinct cells while measuring their effective conductivity (as in Figure 1). It is similar to iso-electric focusing, except that it uses DEP instead of electrophoresis to concentrate cells and particles to the region in a conductivity gradient where their polarization charge vanishes.



▲ Figure 1: IDS microfluidic device used to measure electrical properties of the cells. The spatial conductivity gradient makes cells with different electrical properties pass through the electrodes at different positions (Iso-Dielectric Point - IDP).

Sepsis is an uncontrolled activation of the immune system that causes an excessive inflammatory response. There is an unmet need to develop tools to monitor sepsis progression, which occurs quickly and provides few clues to indicate if treatment is effective. Previously, we have found that the electrical profile of leukocytes changes with activation state. To rapidly measure the electrical profile of leukocytes from whole blood, we have integrated IDS with the spiral inertial microfluidic sorter for leukocyte isolation using an injection loop (see Figure 2a). The spiral inertial sorter minimizes the effect of activation during leukocyte isolating (Figure 2b) and results in depletion of 90% of erythrocytes and recovery of 90% of leukocytes (Figure 2c). This integrated microfluidic system provides a simple assay to monitor sepsis progression in nearly real time.



▲ Figure 2: Integrated IDS system with inertial sorter. (a) A spiral inertial microfluidic sorter isolates leukocytes and stores them in injection loop (Load mode). Injection loop then pushes cells into IDS device for enumeration and electrical characterization (Inject mode). (b) Comparison of leukocyte activation level before input, after spiral sorter, after RBC lysis buffer, and after PMA treatment (positive control). Spiral sorter has smaller effect on activation than RBC lysis buffer. (c) Spiral sorter removes 90 % RBCs; it recovers 90% of WBCs.

FURTHER READING

- M. D. Vahey and J. Voldman, "An Equilibrium Method for Continuous-Flow Cell Sorting Using Dielectrophoresis," *Analytical Chemistry*, vol. 80, no. 9, pp. 3135-3143, 2008.
- H. W. Su, J. L. Prieto, and J. Voldman, "Rapid dielectrophoretic characterization of single cells using the dielectrophoretic spring," *Lab on a Chip*, vol. 13, pp. 4109-4117, 2013.
- L. D. Wu, G. F. Guan, H. W. Hou, A. A. S. Bhagat, and J. Han, "Separation of Leukocytes from Blood Using Spiral Channel with Trapezoid Cross-Section," *Analytical Chemistry*, vol. 84, pp. 9324-9331, Nov. 6, 2012.

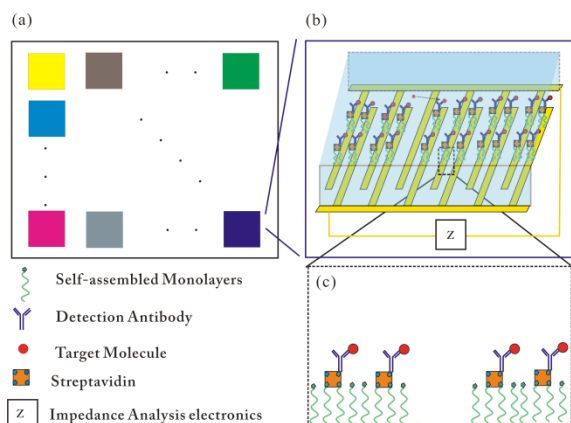
Microfluidic Electronic Detection of Protein Biomarkers

D. Wu, J. Voldman
Sponsorship: Maxim Integrated

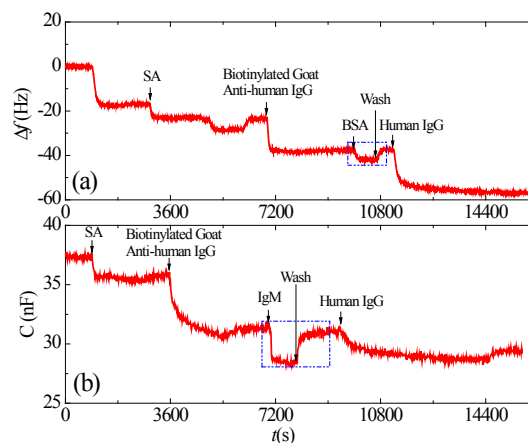
Immunoassays use antibodies to detect protein biomarkers, with a substantial market and significant clinical importance. However, traditional immunoassays are performed in centralized laboratories using optical methods, which means results take days and they cannot be highly multiplexed, in turn increasing patient visits, healthcare costs, and decreasing healthcare outcomes. We are developing all-electronic immunoassays with which we can 1) achieve high-throughput, potentially measuring all protein biomarkers in blood samples; 2) reduce cost by taking advantage of the decreasing cost of silicon electronics; and 3) deliver results to patients before they meet with their physicians.

The biosensor is illustrated in Figure 1: samples are loaded into the microfluidic channel, antigens specifically bind to antibodies on interdigital electrodes (IDEs), and finally the presence of antigens is captured by capacitance change due to the binding. To immobilize antibodies onto IDEs, the surface was modified using self-assembled monolayers and specific binding between

biotin and streptavidin (SA). The surface modification was first tested on gold crystal and characterized using quartz crystal microbalance monitoring with dissipation (QCM-D). As Figure 2(a) shows, the decrease of frequency after introducing SA, antibody [biotinylated goat anti-human Immunoglobulin G (IgG)] and antigen (human IgG) indicated their bindings. The surface also suppressed nonspecific binding because non-specifically attached bovine serum albumin (BSA) was removed by simple washing (as in the rectangle). The surface modification was then applied on the sensor. The capacitance during surface modification was measured [see Figure 2(b)]. The capacitance decrease caused by nonspecific binding [Immunoglobulin M (IgM)] was recovered by washing (as in the rectangle), which was consistent with the QCM-D result that nonspecifically bound proteins were removed by washing. The specific binding of SA, antibody and antigen was correctly revealed by decrease of capacitance and thus validated the electronic detection of protein biomarkers.



▲ Figure 1: (a) Illustration of multiplexed all-electronic biosensors. (b) Illustration of one pixel of the sensor. (c) Cross-section of one pixel.



▲ Figure 2: (a) QCM-D measurement of protein binding to gold crystals; blocking was applied before and washing was applied after introducing SA, antibody, and antigen; the two are not labeled; (b) Electric measurement of protein binding to gold IDEs; washing was also applied after introducing these proteins but is not labeled.

FURTHER READING

- W. Qoronfled and K. Lindpaintner, "Protein biomarker immunoassays: opportunities and challenges," *Drug Discovery World*, 2010 Winter, pp. 19-28, Nov. 2010.
- J. S. Daniels and N. Pourmand, "Label-free Impedance Biosensors: Opportunities and Challenges," *Electroanalysis*, vol. 19, pp. 1239-1257, 2007.

Cell-based Sensors for Measuring Impact of Microsystems on Cell Physiology

A. Fendyur, S. Varma, J. Voldman
Sponsorship: NIH

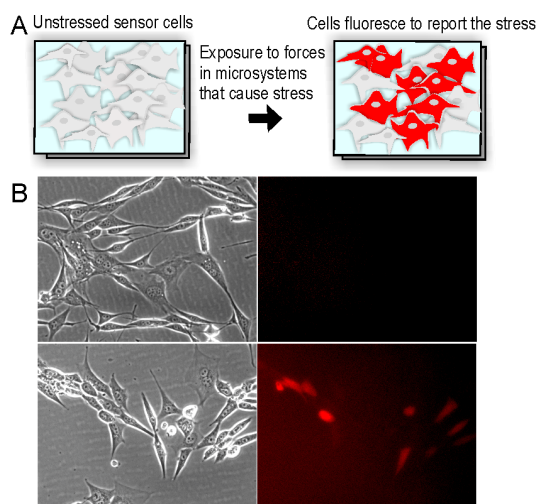
The use of microsystems to study and manipulate cells has rapidly advanced in recent years. However, along with the increase in usage comes a growing concern regarding the toxic impact of such microsystems on cell physiology. DNA damage and heat shock are possible adverse outcomes caused by various forces generated in microsystems. In addition, flows within such systems generate fluid shear stress that may adversely affect cell health as well. In this project, we are developing a set of cell-based fluorescent sensors to measure DNA damage, heat shock and shear-induced stress experienced by cells in microsystems. Toxicity assays using cells, engineered to express fluorescent protein driven by an activation of a molecular pathway offer high-throughput, user-friendly and non-destructive alternative to assess gene expression (see Figure 1a).

To assay DNA damage, we engineered NIH-3T3 cells to fluoresce upon p53-p21-DNA-damage pathway activation by expressing red fluorescent protein (RFP) (see Figure 1b). Creating the shear-stress sensor was challenging because the relevant molecular pathways

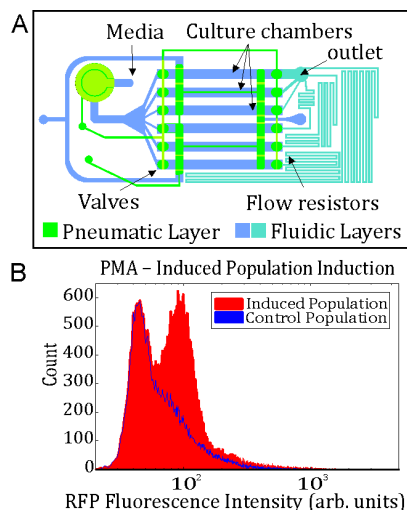
have not been entirely elucidated. We characterized the gene expression profile of NIH-3T3 cells using a multi-flow microfluidic device that can simultaneously apply logarithmic (1000 \times) range of shear stress conditions (as in Figure 2a) and using the qRT-PCR-based approach to identify the shear sensitive genetic node we designed an RFP-reporter plasmid. NIH-3T3 cells were transfected to create shear stress response sensor. We successfully verified our sensor functionality by noting correlating fluorescence response to PMA (chemical inducer of flow shear stress pathway) by flow cytometry (Figure 2b).

For the heat-shock reporting sensor we re-engineered our existing heat shock sensor to express RFP as the activation color, similar to DNA damage and shear stress reporting sensors.

A number of sensors can be combined for multiplexed analysis of multiple stresses at once, as might be experienced in a typical microsystem. Each sensor can be identified by the different constitutive color it expresses.



▲ Figure 1: a) Approach to quantify stress caused by forces generated in microsystems using our sensor. b) DNA damage reporting sensor (upper panel). 24 hrs after DNA damage caused by methyl methanesulfonate - DNA alkylating agent (lower panel), cells fluoresce to report the stress.



▲ Figure 2: a) Perfusion device layout. Cells are seeded in six chambers simultaneously and experience logarithmic shear stress based upon connectivity to fluid flow resistors. b) Histograms of fluorescent intensity of reporter control (blue) and PMA-induced (100 ng/ml) population. The shift towards higher RFP intensity due to PMA proves functionality of designed plasmid and reporters.

FURTHER READING

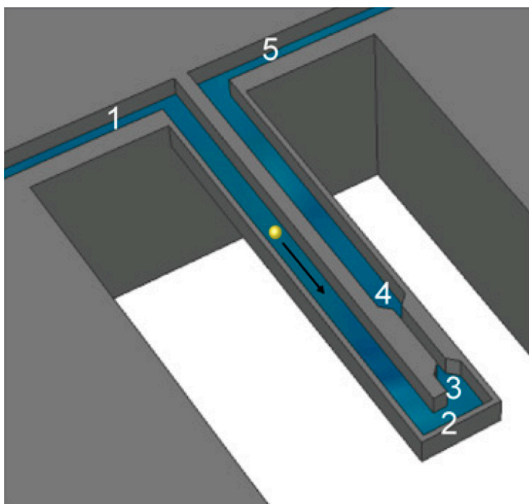
- Y.-C. Toh and J. Voldman, "Fluid shear stress primes mouse embryonic stem cells for differentiation in a self-renewing environment via heparin sulfate proteoglycans transduction," *Faseb Journal*, vol. 25, pp. 1208-17, 2011.
- S. P. Desai and J. Voldman, "Cell-based sensors for quantifying the physiological impact of microsystems," *Integrative Biology*, vol. 3, pp. 48-56, 2011.
- S. P. Desai and J. Voldman, "Measuring the impact of dielectrophoresis on cell physiology using a high-content screening platform" in *Proc. Micro Total Analysis Systems '08*, 2008, pp. 1308-10.

Characterizing Deformability and Surface Friction of Cancer Cells

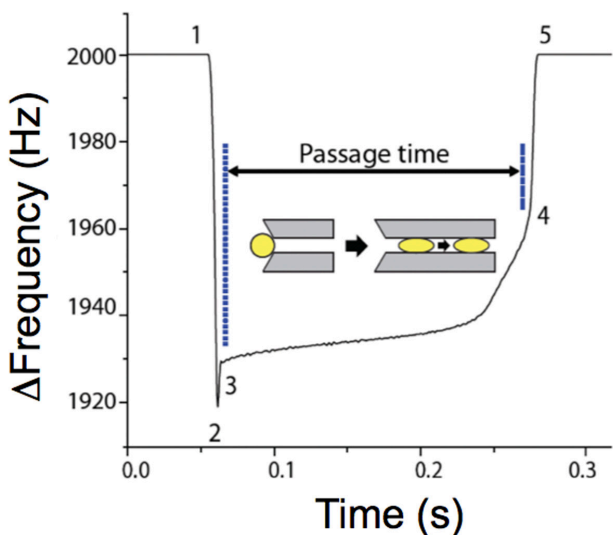
S. Byun, S. Son, D. Amodei, N. Cermak, J. Shaw, J.H. Kang, V.C. Hecht, M. Winslow, T. Jacks, P. Mallick, S.R. Manalis
Sponsorship: NIH

Metastasis requires the penetration of cancer cells through tight spaces, which is mediated by the physical properties of the cells as well as their interactions with the confined environment. Various microfluidic approaches have been devised to mimic traversal in vitro by measuring the time required for cells to pass through a constriction. Although a cell's passage time is expected to depend on its deformability, measurements from existing approaches are confounded by a cell's size and its frictional properties with the channel wall. We developed a device (Figure 1) that enables the precise measurement of: i) the size of a single cell, given by its buoyant mass, ii) the velocity of the cell entering a constricted microchannel (entry velocity) and iii) the velocity of the cell as it transits through the constriction (transit velocity). Changing

the deformability of the cell by perturbing its cytoskeleton primarily alters the entry velocity, whereas changing the surface friction by immobilizing positive charges on the constriction's walls primarily alters the transit velocity, indicating that these parameters can give insight into the factors affecting the passage of each cell. When accounting for cell buoyant mass, we find that cells possessing higher metastatic potential exhibit faster entry velocities than cells with lower metastatic potential. We additionally find that some cell types with higher metastatic potential exhibit greater than expected changes in transit velocities, suggesting that not only the increased deformability but reduced friction may be a factor in enabling invasive cancer cells to efficiently squeeze through tight spaces.



▲ Figure 1a: Suspended microchannel resonator (SMR) with a constriction (6 μm wide, 15 μm deep, and 50 μm long) located at the apex. A cell passing through an embedded microfluidic channel is deformed as it flows into the constriction. Numbers 1-5 indicate different positions within the microchannel to demonstrate the trajectory of a cell flowing inside the channel.



▲ Figure 1b: The resonant frequency response of the SMR as the cell passes through the microfluidic channel. The numbers 1-5 correspond to the position of the cell in the cantilever, as marked in (A). The height of the peak corresponds to the buoyant mass of the cell (1 \rightarrow 2). The cell slows down as it deforms to enter the constriction (entry), and then speeds up as it travels through the constriction (transit). The passage time corresponds to the sum of the entry and transit times (3 \rightarrow 4).

FURTHER READING

- S. Byun, S. Son, D. Amodei, N. Cermak, J. Shaw, J.H. Kang, V.C. Hecht, M. Winslow, T. Jacks, P. Mallick and S.R. Manalis, "Characterizing deformability and surface friction of cancer cells," *Proceedings of the National Academy of Sciences of the United States of America*, vol. 110, pp. 7580-5, 2013.

